

Modeling and assessment of triple-frequency BDS precise point positioning

Fei Guo^{1,2,3} · Xiaohong Zhang^{1,2,3} ·
Jinling Wang⁴ · Xiaodong Ren¹

Received: 5 September 2015 / Accepted: 15 May 2016 / Published online: 14 June 2016
© Springer-Verlag Berlin Heidelberg 2016

Abstract The latest generation of GNSS satellites such as GPS BLOCK-IIIF, Galileo and BDS are transmitting signals on three or more frequencies, thus having more choices in practice. At the same time, new challenges arise for integrating the new signals. This paper contributes to the modeling and assessment of triple-frequency PPP with BDS data. First, three triple-frequency PPP models are developed. The observation model and stochastic model are designed and extended to accommodate the third frequency. In particular, new biases such as differential code biases and inter-frequency biases as well as the parameterizations are addressed. Then, the relationships between different PPP models are discussed. To verify the triple-frequency PPP models, PPP tests with real triple-frequency data were performed in both static and kinematic scenarios. Results show that the three triple-frequency PPP models agree well with each other. Additional frequency has a marginal effect on the positioning accuracy in static PPP tests. However, the benefits of third frequency are significant in situations of where there is poor tracking and contaminated observations on frequencies B1 and B2 in kinematic PPP tests.

Keywords BeiDou Navigation satellite system (BDS) · Precise point positioning (PPP) · Triple-frequency PPP · Multi-GNSS Experiment (MGEX) · Differential code bias (DCB) · Inter-frequency bias (IFB)

1 Introduction

It is well known that the earlier GPS and GLONASS satellites were designed to transmit signals on two frequencies to account for the dispersive part of atmosphere-induced distortions, the so-called ionospheric delays. However, the new generations of Global Navigation Satellite System (GNSS) all operate with three or more frequencies (Feng et al. 2007; Li et al. 2010). As part of the modernization of GPS, newly launched Block-IIIF satellites are now transmitting the third civil signal L5 (1176.45 MHz) in addition to the existing L1 (1575.42 MHz) and L2 (1227.60 MHz) signals (<http://www.gps.gov>). The Europe Galileo system was designed to provide signals in a total of four frequencies centered at E1 (1575.42 MHz), E6 (1278.75 MHz), E5b (1207.14 MHz) and E5a (1176.45 MHz) for commercial and civilian use (<http://www.gsc-europa.eu>). The Chinese BeiDou Navigation Satellite System (BDS) has already launched a regional navigation service since the end of 2012 and continues to develop a global system in the near future (<http://www.beidou.gov.cn>). Currently, a total of 20 operational BDS satellites including five geostationary orbit (GEO), eight inclined geosynchronous orbit (IGSO) and seven medium altitude Earth orbit (MEO) satellites are transmitting triple-frequency signals centered at B1 (1561.098 MHz), B2 (1207.14 MHz), and B3 (1268.52 MHz).

The extra frequencies are expected to benefit precise GNSS data processing, such as carrier phase multipath extraction, cycle slip detection, and especially ambiguity

✉ Xiaohong Zhang
xhzhang@sgg.whu.edu.cn

¹ School of Geodesy and Geomatics, Wuhan University, 129 Luoyu Road, Wuhan 430079, China

² Key Laboratory of Geophysical Geodesy, National Administration of Surveying Mapping and Geoinformation, 129 Luoyu Road, Wuhan 430079, China

³ Collaborative Innovation Center for Geospatial Technology, 129 Luoyu Road, Wuhan 430079, China

⁴ School of Civil and Environment Engineering, UNSW Australia, Sydney, NSW 2052, Australia

resolution. The only known way to extract phase multipath information is through residuals of short baseline processing, since no single-station indicators are available in dual-frequency GNSS. With the third or more frequencies, new approaches to estimate phase multipath from a single-station become available (Simsky 2006). Due to the presence of new frequencies, the traditional approaches dealing with cycle slip problems are expanded to multi-frequency cases (e.g., Dai et al. 2009; Lacy et al. 2012; Zhao et al. 2015; Zhang and Li 2015). As for carrier phase ambiguity resolution (AR), significant research effort has been invested towards GPS and Galileo AR in relative positioning using three or more frequencies, including the earliest studies by Forssell et al. (1997) and Vollath et al. (1998), which described the three carrier phase ambiguity resolution (TCAR) approach. Hatch et al. (2000) and Jung et al. (2000) proposed the cascading integer resolution (CIR) method. However, both the TCAR and CIR were designed for use with the geometry-free model. Teunissen et al. (2002) compared the TCAR, CIR and the least-squares ambiguity decorrelation adjustment (LAMBDA) methods at different levels, proving LAMBDA the optimal method for GNSS AR. Since 2005, a large number of publications have contributed to TCAR issues, and the term TCAR has been extended to use with both the geometry-free and geometry-based models (e.g., Feng and Rizos 2005; Feng 2008; Feng and Li 2009; Li et al. 2010; Tang et al. 2014; Zhang and He 2015). Generally, all the proposed methods aim to shorten the time span necessary for the successful estimation of ambiguities at the correct integer values or to stretch the baseline length for which a successful resolution is possible in real time.

Nevertheless, only a few studies relate to multi-frequency precise point positioning (PPP). One example is that Geng and Bock (2013) proposed a method for triple-frequency PPP ambiguity resolution, and demonstrated its potential to achieve rapid ambiguity resolution with simulated triple-frequency GPS data. However, they still used the traditional dual-frequency model to achieve the final PPP solutions. The triple-frequency PPP model and its performance were not fully investigated. Tegner and Øvstedal (2014) as well as Elsobeiey (2015) also investigated triple carrier precise point positioning using GPS L5. Unfortunately, the number of GPS satellites with triple-frequency signals was quite limited and thus the contribution of third frequency has not been effectively demonstrated. As the only one truly operating triple-frequency navigation system, BDS provides the feasibility to demonstrate the practical performance of triple-frequency PPP. Conventionally, the ionosphere-free carrier phase (and pseudorange) combination is used in dual-frequency PPP. With the third frequency, more combination choices are available and the redundancy of observations is significantly increased. Therefore, the third signal is expected to be beneficial to enhancing the possibilities for the best

positioning. But how much we can benefit from an additional signal is still a major open research topic. At the same time, new challenges arise for processing the new signals, as, for instance, new biases need to be properly handled.

This paper contributes to the modeling and assessment of triple-frequency float PPP with BDS. In Sect. 2, we will first present the mathematical models of triple-frequency PPP with BDS. In particular, new biases as well as parameterizations will be addressed. The Sect. 3 will present the assessment of the triple-frequency PPP models. After a short statement about the data and processing schemes, the positioning performance of both dual- and triple-frequency PPP will be demonstrated in both static and kinematic scenarios. Last, the conclusions will be shown in Sect. 4.

2 Triple-frequency PPP models for BDS

This section presents the mathematical models for triple-frequency PPP with BDS data. After a short description of the general observation model, the ionosphere-free, triple-frequency PPP models, and the uncombined triple-frequency PPP models are developed in detail. We end this section with discussions on the different models.

2.1 General observation model

For a single epoch observation between one satellite and one receiver, the undifferenced (UD) pseudorange P and carrier phase L measurements can be modeled as (Leick 2003; Xu 2007):

$$\begin{aligned} P_{r,n}^s &= \rho_r^s + t_r - t^s + \gamma_n \cdot I_{r,1}^s + T_r^s + d_{r,n} - d_n^s + \varepsilon_{r,n}^s \quad (1) \\ L_{r,n}^s &= \rho_r^s + t_r - t^s - \gamma_n \cdot I_{r,1}^s + T_r^s + \lambda_n \cdot w_r^s + \lambda_n \cdot N_{r,n}^s \\ &\quad + \lambda_n \cdot (b_{r,n} - b_n^s) + \xi_{r,n}^s \quad (2) \end{aligned}$$

where indices s , r , and n refer to the satellite, receiver, and carrier frequency, respectively; ρ_r^s denotes the geometric distance between satellite and receiver; t_r and t^s are the clock biases of receiver and satellite; $I_{r,1}^s$ is the slant ionospheric delay at B1 frequency; γ_n is the ionospheric factor at frequency n ; T_r^s is the tropospheric delay of the signal path; λ_n is the carrier phase wavelength; w_r^s is the phase wind-up delay; $N_{r,n}^s$ is the integer phase ambiguity; $d_{r,n}$ and d_n^s are the code biases of receiver and satellite; $b_{r,n}$ and b_n^s are, respectively, the uncalibrated phase delays (UPDs) for receiver and satellite. $\varepsilon_{r,n}^s$ and $\xi_{r,n}^s$ are the sum of multipath effects and thermal noise for the pseudorange and carrier phase measurements. Note that all variables are expressed in meters; except the ambiguity, UPDs, and phase wind-up delay, which are expressed in cycles.

For convenience, the following notations are defined:

$$\begin{aligned} \gamma_n &= \frac{f_1^2}{f_n^2}, \alpha_{mn} = \frac{f_m^2}{f_m^2 - f_n^2}, \beta_{mn} = -\frac{f_n^2}{f_m^2 - f_n^2}, \text{DCB}_{mn}^s \\ &= d_m^s - d_n^s, \text{DCB}_{r,mn} = d_{r,m} - d_{r,n} \end{aligned} \quad (3)$$

where f_m is the signal frequency ($m, n = 1, 2, 3; m \neq n$); α_{mn} and β_{mn} are frequency factors; DCB_{mn}^s and $\text{DCB}_{r,mn}$ are commonly referred to as the satellite or receiver differential code bias (DCB) between P_m and P_n .

The first order of ionospheric delays can be eliminated by forming linear combination(s) of measurements at different frequencies. Such combination is known as ionosphere-free (IF) combination, which is the most popular model used in PPP. An alternative way is to process the raw measurements where the slant ionospheric delays are estimated as unknowns. Tropospheric delays of the dry component are usually corrected by a priori empirical model, while the zenith wet delays are estimated as unknowns. In addition, the phase center offsets (PCO), relativity effects, as well as Earth tides must also be corrected according to the existing models (Kouba 2009; Petit and Luzum 2010), although they are not included in Eqs. 1 and 2.

Typically, precise orbit and clock products from IGS MGEX (Multi-GNSS Experiment) are used in PPP to remove satellite orbit and clock errors (Dow et al. 2009). By convention, the precise BDS satellite clock corrections are associated to B1/B2 ionosphere-free combination. As such, the precise satellite clock correction (t_{12}^s) contains a specific linear combination of P1 and P2 code biases, that is:

$$t_{12}^s = t^s + (\alpha_{12} \cdot d_1^s + \beta_{12} \cdot d_2^s) \quad (4)$$

The satellite code biases can only be mitigated by forming B1/B2 IF combination, whereas they cannot be cancelled in any other combination. To account for this, satellite DCB products provided by MGEX can be used for compensation according to Guo et al. (2015). For the carrier phase, the uncalibrated phase delays cannot be cancelled and will be mapped into ambiguities. This mapping will not be a problem since the ambiguities are estimated as a lumped term and treated as float values.

With precise satellite orbit, clock and DCB corrections, the corresponding terms can be removed and the pseudorange and carrier phase observation can be simplified as:

$$P_{r,n}^s = \bar{\rho}_{r,P}^s + t_r + \gamma_n \cdot I_{r,1}^s + M_r^s \cdot T_r + d_{r,n} + \varepsilon_{r,n}^s \quad (5)$$

$$L_{r,n}^s = \bar{\rho}_{r,L}^s + t_r - \gamma_n \cdot I_{r,1}^s + M_r^s \cdot T_r + \lambda_n \cdot \bar{N}_{r,n}^s + \xi_{r,n}^s \quad (6)$$

where $\bar{\rho}$ is the same quantity as ρ plus the contribution of satellite clock biases, dry tropospheric delays, phase center offsets, relativistic effects, Earth tides, and phase wind-up

(carrier phase only), etc. M_r^s is the mapping function of wet tropospheric delays; T_r is the zenith tropospheric delay at station r ; $\bar{N}_{r,n}^s$ is the lumped ambiguity term, which is non-integer due to the presence of UPDs:

$$\bar{N}_{r,n}^s = N_{r,n}^s + b_{r,n} - b_n^s \quad (7)$$

With triple-frequency BDS data, a general model of linear combinations can be expressed as (Feng 2008):

$$\begin{aligned} P_{r,(i,j,k)}^s &= i \cdot e_{1,(i,j,k)} \cdot P_{r,1}^s + j \cdot e_{2,(i,j,k)} \cdot P_{r,2}^s \\ &\quad + k \cdot e_{3,(i,j,k)} \cdot P_{r,3}^s \end{aligned} \quad (8)$$

$$\begin{aligned} L_{r,(i,j,k)}^s &= i \cdot e_{1,(i,j,k)} \cdot L_{r,1}^s + j \cdot e_{2,(i,j,k)} \cdot L_{r,2}^s \\ &\quad + k \cdot e_{3,(i,j,k)} \cdot L_{r,3}^s \end{aligned} \quad (9)$$

where i, j , and k ($i, j, k = 0, 1$) are, respectively, the frequency indexes of B1, B2 and B3 signals. A value of zero or one means that signal at the corresponding frequency is excluded from or included for the combination. $e_{n,(i,j,k)}$ ($n = 1, 2, 3$) is the combination coefficient of the n th (frequency) signal. The uncombined model can be regarded as a special case of linear combination model.

2.2 IF-based models

The ionosphere-free (IF) PPP model with triple-frequency measurements can be implemented by the following two means: on the one hand, measurements on triple frequencies could be combined between any of the two frequencies like the dual-frequency ionosphere-free combination. In this case, it will produce three dual-frequency ionosphere-free carrier phase (and pseudorange) combinations (i.e., B1/B2, B1/B3, and B2/B3). We define this model as ‘‘IF-PPP1’’ in this paper. On the other hand, measurements on triple frequencies could be directly combined among three frequencies, in which case only one optimal (i.e., minimum noise) triple-frequency, ionosphere-free carrier phase (and pseudorange) combination (i.e., B1/B2/B3) is obtained. We define such model as ‘‘IF-PPP2’’.

2.2.1 IF-PPP1: ionosphere-free model with two dual-frequency combinations

Applying Eqs. 8,9, we can form three sets of dual-frequency, ionosphere-free combination for the pseudorange among B1, B2 and B3 signals:

$$\begin{bmatrix} P_{r,(1,1,0)}^s \\ P_{r,(1,0,1)}^s \\ P_{r,(0,1,1)}^s \end{bmatrix} = \begin{bmatrix} e_{1,(1,1,0)} & e_{2,(1,1,0)} & 0 \\ e_{1,(1,0,1)} & 0 & e_{3,(1,0,1)} \\ 0 & e_{2,(0,1,1)} & e_{3,(0,1,1)} \end{bmatrix} \begin{bmatrix} P_{r,1}^s \\ P_{r,2}^s \\ P_{r,3}^s \end{bmatrix} \quad (10)$$

Same combination equations hold for the phase observables. The coefficients of the combinations are obtained by imposing the ionosphere-free condition on each combination.

Note that only two of the three sets of IF combination are independent. Considering that the noise amplification factor of the third combination is much larger than the other two, the first two sets of combination, i.e., (1, 1, 0) and (1, 0, 1), are used in this model.

In the case that the receiver hardware delay has a common bias for the dual-frequency IF-PPP (using only B1/B2 or B1/B3), such bias will be absorbed by the receiver clock parameter and thus we do not have to consider it. However, the situation is different for triple-frequency PPP once we use two or more IF combinations (B1/B2 and B1/B3). Since the receiver code biases are different on each IF combination, they cannot be compensated by the receiver clock anymore. To account for this, separate clock parameters should be solved for each IF combination. Alternatively, an inter-frequency bias (IFB, or receiver differential code bias) parameter can be estimated in addition to the receiver clock bias. Here, we introduce an IFB parameter on the B1/B3 code combination. The receiver IFB is considered as common to all satellites. Then, the linearized observation equations can be written as

$$P_{r,(1,1,0)}^s = \mu \cdot X + \bar{t}_r + M_r^s \cdot T_r \tag{11}$$

$$l_{r,(1,1,0)}^s = \mu \cdot X + \bar{t}_r + M_r^s \cdot T_r + B_{r,(1,1,0)}^s \tag{12}$$

$$P_{r,(1,0,1)}^s = \mu \cdot X + \bar{t}_r + M_r^s \cdot T_r + ifb \tag{13}$$

$$l_{r,(1,0,1)}^s = \mu \cdot X + \bar{t}_r + M_r^s \cdot T_r + B_{r,(1,0,1)}^s \tag{14}$$

$$S = [X, \bar{t}_r, T_r, ifb, B_{r,(1,1,0)}^s, B_{r,(1,0,1)}^s]^T \tag{15}$$

where p and l denote the OMC (observation minus computed) values of pseudorange and carrier phase observables; S is the estimates vector; μ is the vector of line of sight. X stands for the three-dimensional coordinates of receiver; ifb is the receiver inter-frequency bias; \bar{t}_r and B_r^s are, respectively, the receiver clock bias and ambiguity estimates (unit: m). Particularly, the estimable receiver clock \bar{t}_r refers to the ionosphere-free clock ($t_{r,12}$), which is based on the P1 and P2 code IF combination.

2.2.2 IF-PPP2: ionosphere-free model with a single triple-frequency combination

Different from the IF-PPP1 model which forms two dual-frequency ionosphere-free combinations (B1/B2, and B1/B3), the IF-PPP2 model directly combines the triple-frequency measurements within one combination (B1/B2/B3), that is,

$$P_{r,(1,1,1)}^s = e_{1,(1,1,1)} \cdot P_{r,1}^s + e_{2,(1,1,1)} \cdot P_{r,2}^s + e_{3,(1,1,1)} \cdot P_{r,3}^s \tag{16}$$

$$L_{r,(1,1,1)}^s = e_{1,(1,1,1)} \cdot L_{r,1}^s + e_{2,(1,1,1)} \cdot L_{r,2}^s + e_{3,(1,1,1)} \cdot L_{r,3}^s \tag{17}$$

Similar to the IF-PPP1 model, the first order of ionospheric delays is expected to be cancelled and the geometric distance should be kept unchanged. However, such two conditions are insufficient to solve for three unknown parameters and further information is required. The coefficients may be various depending on different criteria such as the minimum noise, integer ambiguities, and long wave length. In this contribution, we choose the minimum noise as the additional criterion for the IF-PPP2 model, and thus the combination coefficients can be uniquely determined.

Since all three pseudoranges are combined within the same code observation equation, the receiver hardware delay biases all ranges by a constant which will be eventually absorbed by the receiver clock parameter. Thus, we do not have to consider it (receiver DCB or inter-frequency bias) in this triple-frequency PPP model. The linearized observation equations can be written as:

$$P_{r,(1,1,1)}^s = \mu \cdot X + \bar{t}_r + M_r^s \cdot T_r \tag{18}$$

$$l_{r,(1,1,1)}^s = \mu \cdot X + \bar{t}_r + M_r^s \cdot T_r + B_{r,(1,1,1)}^s \tag{19}$$

$$S = [X, \bar{t}_r, T_r, B_{r,(1,1,1)}^s]^T \tag{20}$$

Different from the IF-PPP1 model, the estimable receiver clock bias \bar{t}_r and phase ambiguity $B_{r,(1,1,1)}^s$ are associated to the (1, 1, 1) ionosphere-free combination (B1/B2/B3).

2.3 Uncombined model

As already mentioned, the uncombined model can be considered as a special case of the combined model, in which the combination coefficients are identity matrices. The uncombined code observation model reads (Schönemann et al. 2011):

$$\begin{bmatrix} P_{r,(1,0,0)}^s \\ P_{r,(0,1,0)}^s \\ P_{r,(0,0,1)}^s \end{bmatrix} = \begin{bmatrix} 1 & 0 & 0 \\ 0 & 1 & 0 \\ 0 & 0 & 1 \end{bmatrix} \begin{bmatrix} P_{r,1}^s \\ P_{r,2}^s \\ P_{r,3}^s \end{bmatrix} \tag{21}$$

Same uncombined equations hold for the phase observables. By applying Eqs. 5 and 6, the observation model can be expanded as:

$$P_{r,(1,0,0)}^s = \bar{\rho}_{r,P}^s + t_{r,12} + (I_{r,1}^s + \beta_{12} \cdot DCB_{r,12}) + M_r^s \cdot T_r + \varepsilon_{r,1}^s \tag{22}$$

$$L_{r,(1,0,0)}^s = \bar{\rho}_{r,L}^s + t_{r,12} - (I_{r,1}^s + \beta_{12} \cdot DCB_{r,12}) + M_r^s \cdot T_r + B_{r,1}^s + \xi_{r,1}^s \tag{23}$$

$$P_{r,(0,1,0)}^s = \bar{\rho}_{r,P}^s + t_{r,12} + \gamma_2 \cdot (I_{r,1}^s + \beta_{12} \cdot DCB_{r,12}) + M_r^s \cdot T_r + \varepsilon_{r,2}^s \tag{24}$$

$$L_{r,(0,1,0)}^s = \bar{\rho}_{r,L}^s + t_{r,12} - \gamma_2 \cdot (I_{r,1}^s + \beta_{12} \cdot \text{DCB}_{r,12}) + M_r^s \cdot T_r + B_{r,2}^s + \xi_{r,2}^s \tag{25}$$

$$P_{r,(0,0,1)}^s = \bar{\rho}_{r,P}^s + t_{r,12} + \gamma_3 \cdot (I_{r,1}^s + \beta_{12} \cdot \text{DCB}_{r,12}) + M_r^s \cdot T_r + \left(\frac{\beta_{12}}{\beta_{13}} \text{DCB}_{r,12} - \text{DCB}_{r,13}\right) + \varepsilon_{r,3}^s \tag{26}$$

$$L_{r,(0,0,1)}^s = \bar{\rho}_{r,L}^s + t_{r,12} - \gamma_3 \cdot (I_{r,1}^s + \beta_{12} \cdot \text{DCB}_{r,12}) + M_r^s \cdot T_r + B_{r,3}^s + \xi_{r,3}^s \tag{27}$$

Unlike the IF-based PPP models, the slant ionospheric delays are treated as unknowns. Note that both the ionospheric delays and differential code biases are frequency dependent. This implies that not all parameters can be unbiasedly estimable due to rank deficiency, but only combinations of them. For dual-frequency PPP (see also Eqs. 22–25), it is well known that the ionospheric delay ($I_{r,1}^s$) and receiver differential code bias ($\text{DCB}_{r,12}$) are perfectly correlated, and they are estimated as lumped terms in general. As for the triple-frequency PPP, the effects of differential code biases on the third pseudorange, however, cannot be completely absorbed into the ionospheric estimate (see Eq. 26). An additional IFB parameter is, therefore, required to compensate for these effects. Eventually, the linearized observation equations can be written as:

$$P_{r,(1,0,0)}^s = \mu \cdot X + \bar{t}_r + \bar{I}_{r,1}^s + M_r^s \cdot T_r \tag{28}$$

$$L_{r,(1,0,0)}^s = \mu \cdot X + \bar{t}_r - \bar{I}_{r,1}^s + M_r^s \cdot T_r + B_{r,1}^s \tag{29}$$

$$P_{r,(0,1,0)}^s = \mu \cdot X + \bar{t}_r + \gamma_2 \cdot \bar{I}_{r,1}^s + M_r^s \cdot T_r \tag{30}$$

$$L_{r,(0,1,0)}^s = \mu \cdot X + t_r - \gamma_2 \cdot \bar{I}_{r,1}^s + M_r^s \cdot T_r + B_{r,2}^s \tag{31}$$

$$P_{r,(0,0,1)}^s = \mu \cdot X + \bar{t}_r + \gamma_3 \cdot \bar{I}_{r,1}^s + M_r^s \cdot T_r + \text{ifb} \tag{32}$$

$$L_{r,(0,0,1)}^s = \mu \cdot X + \bar{t}_r - \gamma_3 \cdot \bar{I}_{r,1}^s + M_r^s \cdot T_r + B_{r,3}^s \tag{33}$$

$$S = [X, \bar{t}_r, T_r, \bar{I}_{r,1}^s, \text{ifb}, B_{r,1}^s, B_{r,2}^s, B_{r,3}^s]^T \tag{34}$$

where

$$\bar{t}_r = t_{r,12} \tag{35}$$

$$\bar{I}_{r,1}^s = I_{r,1}^s + \beta_{12} \cdot \text{DCB}_{r,12} \tag{36}$$

It is noted that the estimable receiver clock bias is equal to that of the IF-PPP1 model. As for the ionospheric delay estimates, it is worth mentioning that they are not the real slant ionospheric delays due to the effects of receiver DCBs. In other words, the ionospheric delay and receiver differential code bias cannot be separated without the help of added information. To separate them, external constraints such as global ionospheric map (GIM) and receiver DCB products from IGS can be used as a priori information.

2.4 Stochastic models

The precision of GNSS (BDS included) satellite measurements can be quantified through either the satellite elevation, the signal-to-noise ratio, or a combination of both (e.g., Wang et al. 2002; Satirapod and Luansang 2008). The common practice is to quantify the precision throughout the satellite elevation angle, which can take several mapping forms such as exponential and trigonometric functions. In this paper, we use an elevation-dependent weighting scheme with a Sine mapping function. Under the assumptions of uncorrelated observations and same a priori noise ($\sigma_1 = \sigma_2 = \sigma_3 = \sigma_0$) in all three carriers, the variance–covariance matrix of the original uncombined observations (e.g., UC-PPP model) can be expressed as:

$$\sum_{\text{UC}} = \begin{bmatrix} \sigma_0^2 & 0 & 0 \\ 0 & \sigma_0^2 & 0 \\ 0 & 0 & \sigma_0^2 \end{bmatrix} = \sigma_0^2 \cdot \mathbf{I} \tag{37}$$

where $\sigma_0 = a/\sin(E)$; a is a constant, which is generally set to be 0.003 m for carrier phase and 0.3–3.0 m for code observations; E is the satellite elevation angle (unit: rad).

Making use of the error propagation law, the covariance matrices for IF-PPP1 and IF-PPP2 models read:

$$\begin{aligned} \sum_{\text{IF-PPP1}} &= A \sum_{\text{UC}} A^T \\ &= \sigma_0^2 \begin{bmatrix} \alpha_{12}^2 + \beta_{12}^2 & \alpha_{12}\alpha_{13} \\ \alpha_{12}\alpha_{13} & \alpha_{13}^2 + \beta_{13}^2 \end{bmatrix} \end{aligned} \tag{38}$$

$$\begin{aligned} \sum_{\text{IF-PPP2}} &= A' \sum_{\text{UC}} A'^T = \sigma_0^2 (e_{1,(1,1,1)}^2 \\ &\quad + e_{2,(1,1,1)}^2 + e_{3,(1,1,1)}^2) \end{aligned} \tag{39}$$

where A and A' are the design matrices (linear combination coefficients) of IF-PPP1 and IF-PPP2 model, respectively. Applying the BDS frequencies, the design matrices and resulting covariance matrices are

$$A = \begin{bmatrix} 2.487 & -1.487 & 0 \\ 2.944 & 0 & -1.944 \end{bmatrix} \tag{40}$$

$$A' = [2.566 \quad -1.229 \quad -0.337] \tag{41}$$

$$\sum_{\text{IF-PPP1}} = \sigma_0^2 \begin{bmatrix} 8.396 & 7.322 \\ 7.322 & 12.446 \end{bmatrix} \tag{42}$$

$$\sum_{\text{IF-PPP2}} = 8.208\sigma_0^2 \tag{43}$$

As shown in Eq. 42, the B1/B2 combination offers a better priori performance than the B1/B3 combination. The off-diagonal elements of covariance matrix are not zeroes indicating that the two sets of combinations (B1/B2 and B1/B3) of IF-PPP1 model are correlated. The correlation

index reaches over 0.7. This high-correlation implies that the off-diagonal elements of the covariance matrix used in least-squares or Kalman filter should not be neglected to perform a correct parameter estimation and to obtain a realistic a posteriori covariance matrix. It is interesting to look into the design matrices in Eqs. 40 and 41. The triple-frequency combination coefficients of IF-PPP2 are close to those of the B1/B2 dual-frequency combination in IF-PPP1, suggesting the lower contribution of the third frequency. Nevertheless, the IF-PPP2 shows smaller combination noise than the conventional B1/B2 combination in IF-PPP1.

2.5 Discussions on the triple-frequency PPP models

Table 1 summarizes the major characteristics of the three triple-frequency PPP models, including the observation used (Obs.), approximate combination coefficients (e_1 , e_2 , and e_3), ionospheric delay factor with respect to $I_{r,1}^s$ (Ion.), noise amplification factor (Noise), and satellite DCB correction terms. For comparison reason, the traditional dual-frequency, ionosphere-free model (named as IF-PPP0) is given as well.

2.5.1 Formulation forms

First, even though the three triple-frequency PPP models are implemented with different forms, the same inputs (i.e., triple-frequency carrier phase and pseudorange measurements) are used for formulation. For the IF-based PPP models, two highly correlated dual-frequency ionosphere-free combinations (B1/B2 and B1/B3) are formed in the IF-PPP1 model, whereas the triple-frequency signals are combined within one optimal ionosphere-free carrier phase (and pseudorange) combination (B1/B2/B3) in the IF-PPP2 model. As for the UC-PPP model, three raw carrier phase (and pseudorange) measurements are processed directly without combination. Note that the IF-PPP1 and UC-PPP models are more flexible than the IF-PPP2 model in the absence of a particular frequency. By comparing the combination coefficients of the IF-PPP1 and IF-PPP2 models, we can find that the IF-PPP2 model is more like a B1/B2

dual-frequency PPP model due to the lower contribution of the third frequency. But the observation noise of the IF-PPP2 model is slightly smaller than that of the IF-PPP0 and IF-PPP1 models.

2.5.2 Inter-frequency biases

The current precise satellite clock corrections are conventionally associated to P1/P2 code IF combination. To make use of and keep compatible with the precise clock products, inter-frequency biases should be taken into account for all the three triple-frequency PPP models. Satellite differential code biases can be corrected in advance using MGEX DCB products. As for the receiver end, such code biases can be absorbed by receiver clock bias parameter in the IF-PPP2 model, and thus we do not have to consider them. However, an additional IFB parameter should be introduced to compensate for this in the other two models due to their different effects on different frequency bands. Equations 44 and 45 show the IFB estimates of the IF-PPP1 and UC-PPP models, respectively. When it comes to carrier phases, the inter-frequency biases will not be a problem since they can be absorbed by the ambiguity estimates, which are estimated as lumped terms and treated as float values.

$$ifb_{IF-PPP1} = \beta_{12} \cdot DCB_{r,12} - \beta_{13} \cdot DCB_{r,13} \tag{44}$$

$$ifb_{UC-PPP} = \frac{\beta_{12}}{\beta_{13}} DCB_{r,12} - DCB_{r,13} \tag{45}$$

2.5.3 Estimable parameters

As to the estimates, receiver coordinates and wet tropospheric delays can be regarded as model independent. The other estimates i.e., receiver clock bias, inter-frequency bias, ionospheric delay, as well as ambiguities, however, are associated with a particular model or combination. Inter-frequency bias and ionospheric delay parameters are not always necessary for the three PPP models. The ionospheric delay parameters are cancelled in the IF-based PPP models, and the inter-frequency bias parameter disappears in the

Table 1 Comparisons of the dual- and triple-frequency PPP models

Model	Obs.	e_1	e_2	e_3	Ion.	Noise	DCB correction terms
IF-PPP0	B1/B2	2.487	-1.487	0	0	2.90	0
IF-PPP1	B1/B2	2.487	-1.487	0	0	2.90	0
	B1/B3	2.944	0	-1.944	0	3.53	$\beta_{12} \cdot DCB_{12}^S - \beta_{13} \cdot DCB_{13}^S$
IF-PPP2	B1/B2/B3	2.566	-1.229	-0.337	0	2.86	$(\beta_{12} - e_2) \cdot DCB_{12}^S - e_3 \cdot DCB_{13}^S$
UC-PPP	B1	1	0	0	1	1	$\beta_{12} \cdot DCB_{12}^S$
	B2	0	1	0	1.672	1	$-\alpha_{12} \cdot DCB_{12}^S$
	B3	0	0	1	1.514	1	$-\alpha_{12} \cdot DCB_{13}^S - \beta_{12} \cdot DCB_{23}^S$

IF-PPP2 model. Moreover, the estimation values may be different among three models, even though they are designed as the same parameter. Take the receiver clock bias for example, the estimable clocks of IF-PPP1 and UC-PPP are referred to as P1/P2 ionosphere-free clock ($t_{r,12}$), whereas the estimated receiver clock of IF-PPP2 is the combined effect of $t_{r,12}$ and receiver hardware delays (shown in Eq. 46). The ambiguity estimates are also associated with different frequencies (or coupled frequencies).

$$\begin{aligned} \bar{t}_{r(\text{IF-PPP2})} = t_r + \sum_{n=1}^3 (e_n \cdot d_{r,1}) = t_{r,12} \\ + (e_2 - \beta_{12}) \cdot \text{DCB}_{r,12} + e_3 \cdot \text{DCB}_{r,13} \end{aligned} \quad (46)$$

2.5.4 Equivalence analysis

Despite of the above-mentioned differences, we should be aware that eliminating nuisance parameters through linear combinations is actually equivalent to explicitly estimating those parameters (Lindlohr and Wells 1985; Schaffrin and Grafarend 1986). Xu (2007) documented the equivalence properties between uncombined and combining algorithms by algebraic linear transformations. It has been proved that both the solution vector and the variance–covariance matrix are identical no matter which algorithms are used (Xu 2007). Obviously, the IF-PPP1 and IF-PPP2 models used in this paper can be obtained by carrying out a related linear transformation to the original equations (i.e., UC-PPP model). Theoretically, all the three PPP models are equivalent as long as the weight matrix (or variance–covariance matrix) is similarly transformed according to the law of covariance propagation. Although different models can lead to a more effective (or easier) dealing of related specific problems, none of the model will lead to better solutions or better precisions of the solutions than the others. Solving the ionosphere-free equations or raw observation equations will lead to the same results.

However, it is worth mentioning that the IF combined and UC models will lead to different results if a priori information (e.g., constant or random-walk process) is added on the ionosphere and inter-frequency bias parameters. In other words, the IF-PPP and UC-PPP models are equivalent only when the estimable ionospheric delays as well as inter-frequency biases are treated as white noise process. Otherwise, additional information would then have an impact on their solutions.

3 Positioning performance evaluation

In this section, a few MGEX stations were used for both static and simulated kinematic PPP tests to verify the triple-

frequency PPP models. Besides, a ship-borne kinematic PPP test was performed to test the triple-frequency PPP performances in real dynamic scenarios. For each test, the positioning accuracy (i.e., epoch-wise position error and root mean squares, RMS) was evaluated. Additionally, the inter-frequency bias and ionospheric delay estimates were analyzed in static PPP tests.

3.1 Data sets and processing strategy

To guarantee adequate number of tracked BDS satellites, six Asia-Pacific regional distributed MGEX stations (namely CUT0, KARR, MRO1, XMIS, GMSD, and JFNG) equipped with Trimble NetR9 receivers were selected to demonstrate the performance of triple-frequency PPP models. Observations in February 2014 (DOY 032-059) and in May 2015 (DOY 121-151) were selected as the core data sets for this study. These MGEX stations were used for both static and simulated kinematic PPP solutions. Moreover, a set of ship-borne kinematic data was used to test the triple-frequency PPP models in real dynamic scenarios.

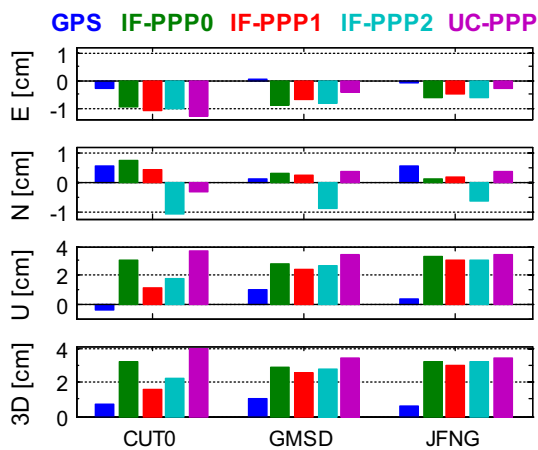
Table 2 summarizes the detailed processing strategy for BDS PPP. Precise orbit and clock products at intervals of 15 and 5 min, respectively, provided by MGEX (e.g., GFZ) were used. A triple-frequency PPP engine based on Kalman filter has been implemented as a new module in TriP software (Zhang et al. 2006). For comparison, the traditional dual-frequency PPP (IF-PPP0), which uses only B1/B2 combination, was also conducted in the following sections. Moreover, GPS PPP solutions based on L1/L2 ionosphere-free combinations were performed and compared with BDS PPP. It is worth mentioning that the coordinates of the MGEX stations are known and have an accuracy of a few millimeters. As for the ship-borne kinematic PPP tests, the coordinate estimations were compared with those of double differencing real-time kinematic (RTK).

3.2 Static PPP tests

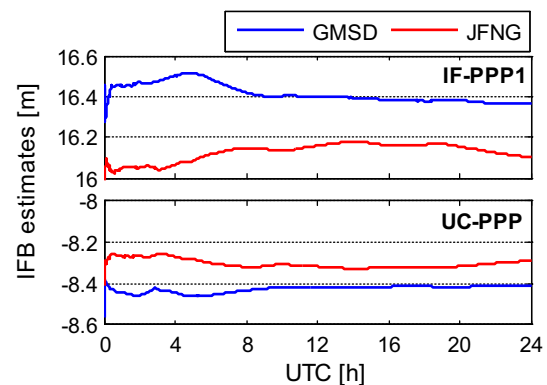
Take day of year (DOY) 047/2014 as a case study, Fig. 1 shows the static positioning errors of CUT0, GMSD, and JFNG in the east (E), north (N), and up (U) components, as well as the three-dimensional (3D) positioning accuracy. By comparing the results of dual-frequency PPP between GPS and BDS, we can find that the horizontal positioning performance of both are comparable to each other with an accuracy of a few millimeters. However, the vertical positioning accuracy of BDS is worse than that of GPS by a factor of three or more. A systematic bias of 2–3 cm can be observed on almost all the BDS-based PPP solutions. This is reasonable when we acknowledge the following two facts. On the one hand, the precision of BDS satellite orbits and clock corrections is worse than that of GPS. On the other

Table 2 BDS PPP processing strategy

Items	Models
Involved solution	B1/B2 Ionosphere-free PPP (IF-PPP0); IF-PPP1; IF-PPP2; UC-PPP
Estimator (engine)	Kalman filter, TriP software (Zhang et al. 2006)
Observations	carrier phase and code observations
Sampling rate	30 s
Elevation cutoff	10°
Weighting scheme	Elevation-dependent weight; 3 mm and 3 m for raw phase and code, respectively
Ionospheric delay	IF-PPP0, IF-PPP1 and IF-PPP2: eliminated by Ionosphere-free combination(s); UC-PPP: estimated as white noise process ($1 \times 10^4 \text{ m}^2$)
Tropospheric delay	Dry component: corrected with GPT model (Boehm et al. 2007) wet component: estimated as random-walk process ($1 \text{ cm}^2/\text{h}$), GMF mapping function
Relativistic effect	Applied
Station displacement	Corrected by IERS Convention 2010, including Solid Earth tide and ocean tide loading (Petit and Luzum 2010)
Satellite antenna phase center offset	Corrected with conventional PCO values from MGEX (Rizos et al. 2013)
Receiver antenna phase center offset	Not applied due to the lack of receiver PCO values for BDS
Phase-wind-up effect	Corrected (Wu et al. 1993)
Satellite differential code bias	Corrected with MGEX DCB products for satellites (Guo et al. 2015); receiver DCBs are absorbed by receiver clock biases or estimated as unknowns
Receiver inter-frequency bias	IF-PPP0/IF-PPP2: absorbed by receiver clock biases IF-PPP1/UC-PPP: estimated as constant
Receiver clock	Estimated as white noise process ($1 \times 10^4 \text{ m}^2$)
Station coordinate	Kinematic PPP: estimated as white noise process ($1 \times 10^4 \text{ m}^2$) Static PPP: estimated as constants
Phase ambiguities	Estimated, constant for each pass; float value

**Fig. 1** Static positioning error of the dual-frequency (GPS and IF-PPP0) and triple-frequency PPP (IF-PPP1, IF-PPP2, and UC-PPP) models on CUT0, GMSD, and JFNG stations (DOY 047/2014)

hand, the current BDS constellation consists mostly of GEO and IGSO satellites, resulting in a poorer geometry (larger PDOP) of BDS observations compared to GPS. Comparing the results of BDS between dual- and triple-frequency PPP, it can be found that solutions of the IF-PPP0, IF-PPP1, IF-PPP2 and UC-PPP agree well with each other in general. The positioning errors are mostly within 1 cm in horizontal

**Fig. 2** Receiver inter-frequency bias (IFB) estimates of the triple-frequency PPP (IF-PPP1 and UC-PPP) models on GMSD, JFNG. (DOY 047/2014)

and 2–3 cm in vertical for both the dual- and triple-frequency PPP models. The triple-frequency PPP model IF-PPP1 shows slightly better performance than the other models.

As the by-products of triple-frequency PPP, the receiver inter-frequency bias estimates are shown in Figs. 2 and 3. Figure 2 shows the epoch-wise IFB estimates of IF-PPP1 and UC-PPP models on GMSD and JFNG stations. The IFB estimate reaches over 16 m for the IF-PPP1, and -8 m for the UC-PPP model. This implies that the IFB estimate of

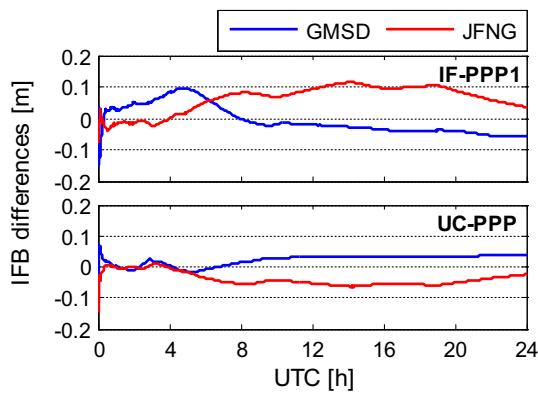


Fig. 3 Differences of the receiver inter-frequency bias (IFB) estimates with respect to the reference IFB values calculated from MGEX DCB products (DOY 047/2014)

IF-PPP1 is about twice that of UC-PPP but opposite sign. It is not surprising if we compare the combination coefficients between Eqs. 44 and 45. This further confirms our derivation of the estimable IFB parameters and their relationship between IF-PPP1 and UC-PPP models. Despite of the large values of IFB, they are stable enough in a single day and thus makes it possible to model the IFB as constants. To verify our IFB estimates, receiver DCBs (i.e., DCB_{12} and DCB_{13}) extracted from the MGEX products were used to calculate the reference IFBs according to Eqs. 44 and 45. Figure 3 shows the differences of our IFB estimates with respect to the reference IFB values. It can be seen that most of their differences are within 0.1 m, indicating that our IFB estimates have an accuracy of a few centimeters.

3.3 Simulated kinematic PPP tests

3.3.1 Dual-frequency PPP (BDS VS GPS)

The same data as used in static PPP tests were reprocessed in kinematic mode i.e., the receiver coordinates were modeled as white noise process. Figure 4 shows the epoch-wise positioning error on CUT0 and JFNG stations using L1/L2 and B1/B2 ionosphere-free combinations. The plots in Fig. 4 show that GPS positioning errors are mostly within 5 cm in the east and north directions, 10 cm in the up direction after a short time convergence. The root mean squares (RMS) of GPS positioning error reach 2–3 cm in horizontal and 4–5 cm in vertical. For BDS, the positioning performance is worse than GPS as expected due to the poor geometry, inaccurate model as well as the limited accuracy of the orbit and clock products available within the current study (Montenbruck et al. 2013; Li et al. 2014). Nevertheless, an accuracy of 3–4 cm in horizontal and 8–10 cm vertically is achievable with the current BDS constellation.

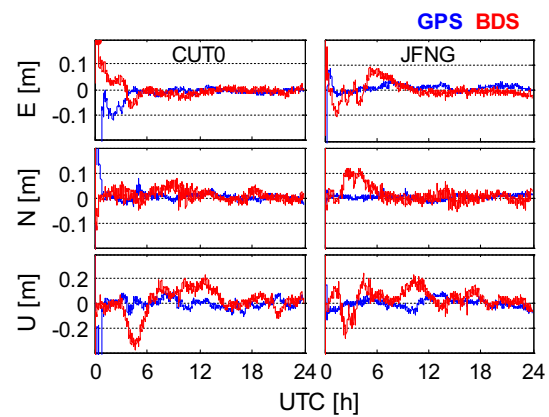


Fig. 4 Comparisons of the BDS/GPS kinematic positioning performance with dual-frequency data (DOY 047/2014)

3.3.2 Triple-frequency PPP (IF-PPP1 VS IF-PPP2 VS UC-PPP)

Figure 5 shows the positioning errors of the triple-frequency PPP models on three representative stations, and the RMS of all selected MGEX stations are summarized in Table 3. It is worth mentioning that solutions of the first half-hour were not involved in statistics considering that they are not converged yet. As shown in Fig. 5, solutions from all the three models perform similarly, suggesting good consistency among the triple-frequency PPP models. Statistics in Table 3 show RMSs of 2–4, 2–3, and 8–10 cm in the east, north, and up directions, respectively, for all the three triple-frequency PPP models and all the stations except for GMSD. Compared to the UC-PPP model, solutions of the IF-PPP1 and IF-PPP2 models show even much better agreements since they both are based on ionosphere-free combinations and have similar noise level. These differences between the IF-based and uncombined PPP models mainly lie in the initial time and re-

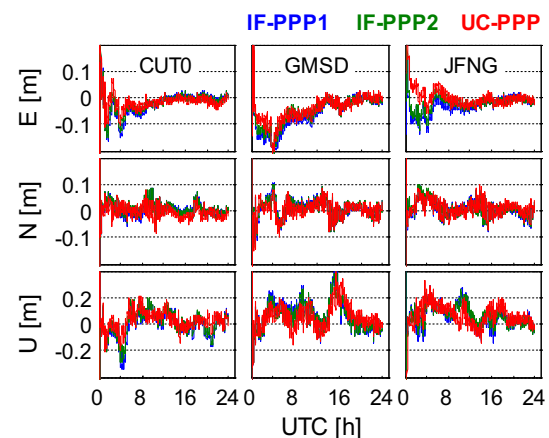
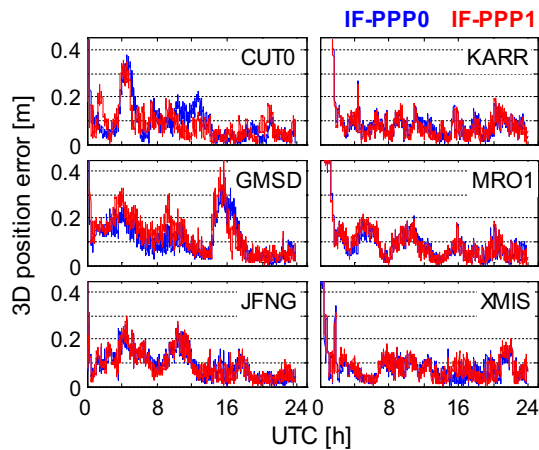


Fig. 5 Comparisons of the kinematic positioning error among triple-frequency PPP models (DOY 047/2014)

Table 3 The RMS of simulated kinematic positioning errors for the different PPP models (unit: cm)

RMS	East			North			Up		
	IF-PPP1	IF-PPP2	UC-PPP	IF-PPP1	IF-PPP2	UC-PPP	IF-PPP1	IF-PPP2	UC-PPP
CUT0	4.5	3.8	2.8	2.1	2.2	2.0	9.4	8.9	6.9
GMSD	8.5	7.3	6.4	3.2	3.0	2.8	12.5	11.8	10.4
JFNG	4.1	3.2	2.9	2.8	2.9	2.7	9.5	9.5	9.7
KARR	2.2	2.1	2.6	2.4	2.5	3.3	7.1	7.3	8.5
MRO1	1.4	1.3	1.8	2.1	2.0	2.7	8.9	8.5	10.1
XMIS	0.2	1.9	1.9	1.8	1.9	1.9	7.8	7.1	8.1

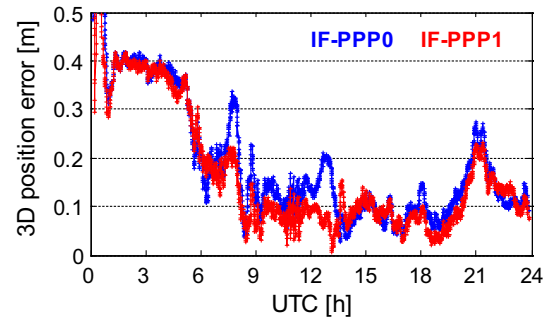
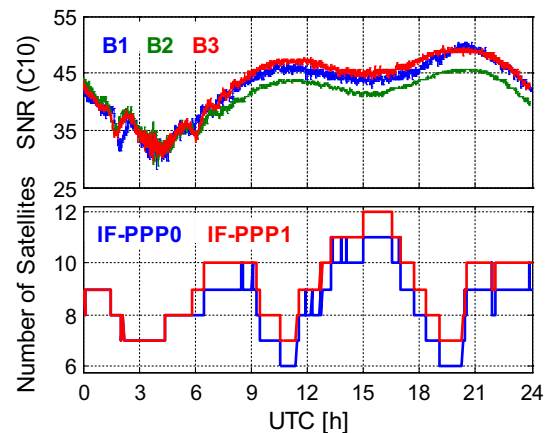
**Fig. 6** Comparisons of the kinematic positioning error among triple-frequency PPP and dual-frequency PPP models (DOY 047/2014: CUT0, GMSD, and JFNG; DOY 118/2015: KARR, MRO1, and XMIS)

initialization stages and can be attributed to the differences in parameterization, as well as noise level. Nevertheless, such small differences can be neglected for kinematic applications.

3.3.3 Benefits of the third frequency (IF-PPP0 VS IF-PPP1)

Take the IF-PPP0 and IF-PPP1 for example, Fig. 6 shows the 3D positioning error of dual- and triple-frequency PPP tests. By comparing the results between dual- and triple-frequency PPP, we can find that the 3D positioning errors agree well with each other within a few millimeters for most of the time. Such small differences implies that the contribution of the third frequency signal is not obvious under the same conditions of geometry and signal strength (quality).

However, the benefits of third frequency would be significant in the presence of poor tracking and contamination on frequencies B1 and B2. To demonstrate this scenario, some typical examples are presented in Figs. 7, 8, 9 and 10. As shown in Fig. 7, the IF-PPP0 and IF-PPP1 show almost the same positioning accuracy at the first 6 h. However, the positioning accuracy of IF-PPP0 is significantly worse than that

**Fig. 7** 3D positioning error of the dual-frequency and triple-frequency PPP on KARR (DOY 150/2015)**Fig. 8** SNR and number of satellites for the triple-frequency PPP on KARR (DOY 150/2015)

of IF-PPP1, particularly during the period of UTC 6–15. The differences of 3D positioning estimates reach over 10 cm. The poor performance of IF-PPP0 is related to the weak signal strength on B2 for C10 satellite as shown in Fig. 8. We can find that the SNR (signal-to-noise ratio) of C10 (an MEO) satellite on B2 frequency becomes obviously smaller than the other two frequencies since about UTC 6 on KARR. As a consequence, loss of lock occurs on B2 signal, reducing the number of available satellites for the IF-PPP0 model. Fortunately, measurements on B1 and B3 frequencies can still

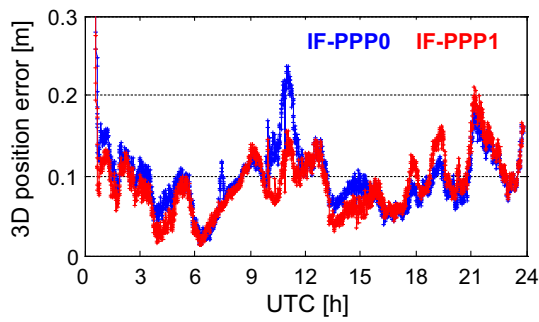


Fig. 9 3D positioning error of triple-frequency PPP and dual-frequency PPP on JFNG station (DOY 146/2015)

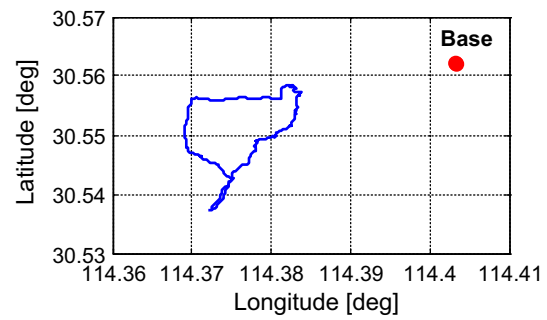


Fig. 11 Location of the base station and the trajectory of the moving carrier (DOY 080/2015)

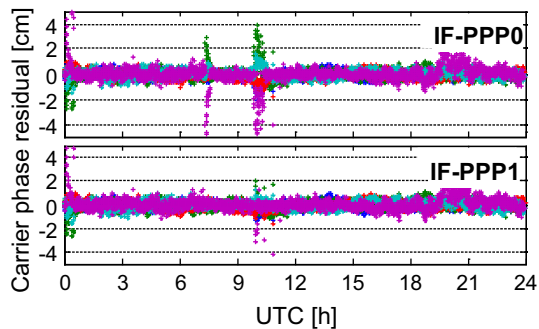


Fig. 10 Carrier phase residuals of the dual- and triple-frequency PPP on JFNG station (DOY 146/2015)

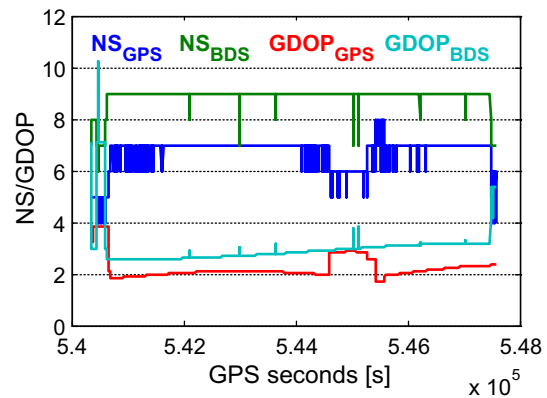


Fig. 12 Number of satellites and GDOP of the ship-borne kinematic data (DOY 080/2015)

be used to enhance the geometry and redundancy once the IF-PPP1 model is applied. Consequently, the third frequency signal improves the positioning accuracy and reliability.

Another example is shown in Figs. 9 and 10. As shown in Fig. 9, the 3D positioning errors of IF-PPP1 are smaller than those of IF-PPP0, particularly during the periods of UTC 7:21–7:26 and 9:53–11:30. The difference of positioning estimates between these two models reaches 5–10 cm during these periods. The reason for this is the unexpected outliers, e.g., gross errors and cycle slips that are unfortunately not effectively detected with B1 and B2 measurements. These outliers will eventually bias the estimates and be reflected in residuals as shown in Fig. 10. However, with the third frequency, more combinations can be used for preprocessing, leading to a higher quality control level. Finally, a more accurate and reliable solutions can be achieved.

3.4 Ship-borne kinematic PPP tests

For this purpose, 2 h of ship-borne BDS/GPS data were collected at Donghu Lake near Wuhan University on March 21, 2015 (DOY 080). The data have a frequency of 1 Hz and cutoff elevation angle of 10°. Parallel to the PPP tests, a base station at a known control point was installed to allow qualitative and quantitative assessment of PPP results through the use of double difference (DD) software, GrafNav. ComNav

receivers were used at both the rover and base stations. Figure 11 shows the trajectory of moving carrier, and the satellite visibility and geometry during this period are depicted in Fig. 12. The distance between the base and rover receivers is about 4 km. During this test, DD ambiguity fixing was successful for most of the epochs, providing positioning accuracy better than 10 cm.

Similarly, both the BDS dual- and triple-frequency PPP models were tested with this data set. GPS dual-frequency PPP solutions were included as well. Figure 13 shows the consistency between PPP and DD solutions. The RMS statistics of all the involved results are summarized in Table 4. It should be noted that the RMS statistics are based on the latter 1.5 h solutions because the first half-hour are not converged yet. As depicted in Fig. 13, GPS dual-frequency PPP shows the worse agreement with the DD results, particularly in the east and up directions. The RMS of their differences reach 8.4 cm in the north, 32.0 cm in the east, and 26.7 cm in the up directions. Such poor performance can be attributed to the limited number of visible satellites as can be seen in Fig. 12. As for the BDS-based PPP, an average number of 9 satellites is available for most of the time. They have good consistencies with the DD results. Statistics in Table 4 suggest an accuracy of 5–6 cm for the north, and 13–15 cm

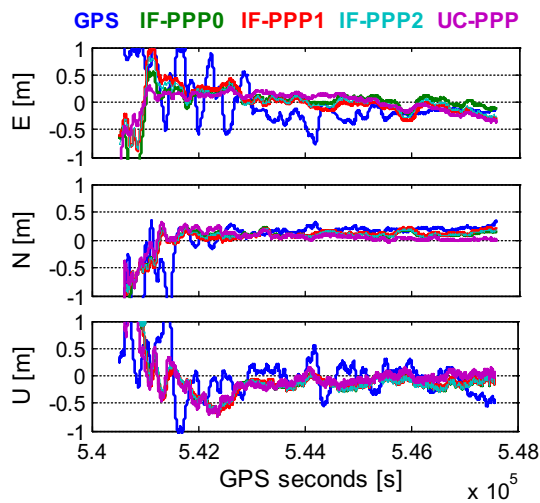


Fig. 13 Kinematic positioning errors of both the dual- and triple-frequency PPP models (DOY 080/2015)

Table 4 The RMS of real kinematic positioning errors for the different PPP models (unit: cm)

	GPS	IF-PPP0	IF-PPP1	IF-PPP2	UC-PPP
East	32.0	13.6	13.5	13.6	13.2
North	8.4	5.5	5.6	5.1	4.4
Up	26.7	14.9	15.0	15.3	15.0

for the east and up components. By comparing the results between BDS dual- and triple-frequency PPP, we can find that they all agree well with each other after convergence. To investigate the benefits of the third frequency at the initial stage, Fig. 14 illustrates the convergence behavior of the IF-PPP0 and IF-PPP1 models. As shown in Fig. 14, the triple-frequency PPP converges faster and runs much more stable than the dual-frequency PPP. This is particularly pronounced in the east direction. Therefore, it can be concluded that PPP will benefit from the increasing number of signals in terms of positioning accuracy and robustness, particularly at the initial stage.

4 Summary and conclusions

To fully exploit the triple-frequency BDS signals, this paper contributed to the modelling and assessment of triple-frequency precise point positioning with BDS data. Three triple-frequency PPP models namely “IF-PPP1”, “IF-PPP2”, and “UC-PPP” were developed. The former two models use ionosphere-free combination(s), and the latter one employs the raw measurements. With the third frequency, receiver inter-frequency biases arise that need to be taken into account in triple-frequency PPP. The observation model and stochas-

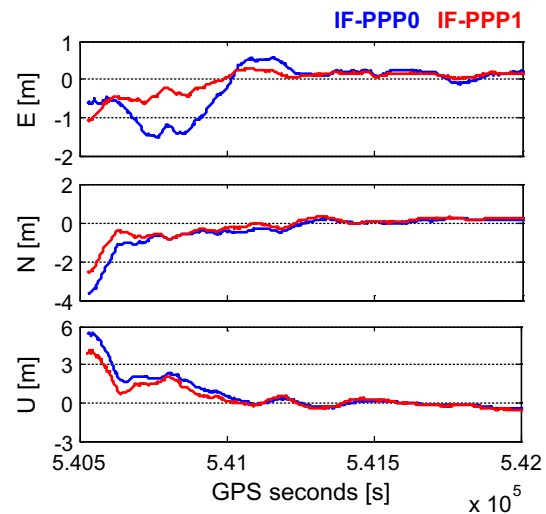


Fig. 14 Comparisons of the convergence performance (results of the first 25 min) between dual- and triple-frequency PPP models

tic model were extended to accommodate the third frequency. The relationship between different models was then discussed in detail.

To demonstrate the triple-frequency PPP models, first, a few MGEX stations located in Asia-Pacific region were used for static and simulated kinematic PPP tests. For comparison, the traditional dual-frequency PPP model with GPS and BDS data was tested as well. Comparative analyses show that both dual- and triple-frequency static PPP can reach an accuracy of a few millimeters in horizontal. Such an accuracy is comparable to that of GPS PPP. However, the vertical positioning accuracy is significantly worse than GPS and shows systematic biases of 2–3 cm. In addition, the estimated inter-frequency biases and ionospheric delays are shown and analyzed. Then, the same static data were used for simulated kinematic PPP tests. In this case, an accuracy of 3–4 cm in horizontal and 8–10 cm vertically is achievable with the current BDS constellation. Such an accuracy is worse than GPS by a factor of two due to its poorer geometry and worse orbit and clock quality. By comparing the results among three triple-frequency PPP models, they have shown very good consistencies. Compared to dual-frequency PPP, the benefits of third frequency would be significant in situations where there is poor tracking and contaminated observations on frequencies B1 and B2. This implies a stronger robustness for the triple-frequency PPP. Finally, a ship-borne kinematic data set was used to test the triple-frequency PPP models in real dynamic scenarios. Results show that the positioning performance is enhanced with the third frequency signals. After convergence, both the dual- and triple-frequency PPP reach an accuracy of better than 0.2 m.

The performance of BDS dual- and triple-frequency PPP is expected to be further improved with more accurate BDS

orbit and clock products and additional BDS MEO satellites in orbit in the future. We should acknowledge that only float PPP solutions are considered in this paper. Investigations on triple-frequency PPP with ambiguity resolution should be addressed in the future.

Acknowledgments The authors gratefully acknowledge IGS Multi-GNSS Experiment (MGEX) for providing GNSS data and products. We appreciate anonymous reviewers for their valuable comments and improvements to this manuscript. Thanks also go to the National Natural Science Foundation of China (No: 41404006, No: 41474025) and the Open Research Fund of State Key Laboratory of Information Engineering in Survey, Mapping and Remote Sensing (No. 15P02).

References

- Boehm J, Heinkelmann R, Schuh H (2007) Short note: a global model of pressure and temperature for geodetic applications. *J Geod* 81(10):679–683. doi:10.1007/s00190-007-0135-3
- Dai Z, Knedlik S, Loffeld O (2009) Instantaneous triple-frequency GPS cycle-slip detection and repair. *Int J Navig Obs*. Article ID 407231: doi:10.1155/2009/407231
- Dow JM, Neilan RE, Rizos C (2009) The international GNSS service in a changing landscape of global navigation satellite systems. *J Geod* 83:191–198. doi:10.1007/s00190-008-0300-3
- Elsobeiey M (2015) Precise point positioning using triple-frequency GPS measurements. *J Navig* 68(3):480–492. doi:10.1017/S0373463314000824
- Feng Y (2008) GNSS three carrier ambiguity resolution using ionosphere-reduced virtual signals. *J Geod* 82(12):847–862. doi:10.1007/s00190-008-0209-x
- Feng Y, Li B (2009) Three carrier ambiguity resolutions: generalized problems, models and solutions. *J Glob Position Syst* 8(2):115–123. doi:10.5081/jgps.8.2.115
- Feng Y, Rizos C (2005) Three carrier approaches for future global, regional and local GNSS positioning services: concepts and performance perspectives. In: *Proceedings of ION GNSS-2005*, pp 2277–2787, Long Beach, CA, 13–16 September
- Feng Y, Rizos C, Higgins M (2007) Impact of multiple frequency GNSS signals on future regional GNSS services. *IONSS Symposium 2007*, Sydney, Australia, 4–6 December
- Forsell B, Martin-Neira M, Harris R (1997) Carrier phase ambiguity resolution in GNSS-2. In: *Proceedings of ION GPS-97*, pp 1727–1736, Kansas City, MO, 16–19 September
- Geng J, Bock Y (2013) Triple-frequency GPS precise point positioning with rapid ambiguity resolution. *J Geod* 87(5):449–460. doi:10.1007/s00190-013-0619-2
- Guo F, Zhang X, Wang J (2015) Timing group delay and differential code bias corrections for BeiDou positioning. *J Geod* 89(5):427–445. doi:10.1007/s00190-015-0788-2
- Hatch R, Jung J, Enge P, Pervan B (2000) Civilian GPS: the benefits if three frequencies. *GPS Solut* 3(4):1–9. doi:10.1007/PL00012810
- Jung J, Enge P, Pervan B (2000) Optimization of cascade integer resolution with three civil GPS frequencies. In: *Proceedings of the ION GPS-2000*, pp 2191–2200, Salt Lake City, UT, 19–22 September
- Kouba J (2009) A guide to using international GNSS service (IGS) products. <http://igsceb.jpl.nasa.gov/igsceb/resource/pubs/UsingIGSProductsVer21.pdf>
- Lacy M, Reguzzoni M, Sanso F (2012) Real-time cycle slip detection in triple-frequency GNSS. *GPS Solut* 16(3):353–362. doi:10.1007/s10291-011-0237-5
- Leick A (2003) *GPS satellite surveying*, 3rd edn. Wiley, New York
- Li B, Feng Y, Shen Y (2010) Three carrier ambiguity resolution: distance-independent performance demonstrated using semi-generated triple frequency GPS signals. *GPS Solut* 14(2):177–184. doi:10.1007/s10291-009-0131-6
- Li M, Qu L, Zhao Q, Guo J, Su X, Li X (2014) Precise point positioning with the BeiDou navigation satellite system. *Sensors* 14(1):927–943. doi:10.3390/s140100927
- Lindlöh W, Wells D (1985) GPS design using undifferenced carrier beat phase observations. *Manuscr Geod* 10(4):255–295
- Montenbruck O, Hauschild A, Steigenberger P, Hugentobler U, Teunissen P, Nakamura S (2013) Initial assessment of the COMPASS/BeiDou-2 regional navigation satellite system. *GPS Solut* 17(2):211–222. doi:10.1007/s10291-012-0272-x
- Petit G, Luzum B (2010) *IERS Conventions 2010 (IERS Technical Note No. 36)*. Verlag des Bundesamts für Kartographie und Geodäsie, Frankfurt am Main, p 179. ISBN:3-89888-989-6
- Rizos C, Montenbruck O, Weber R, Neilan R, Hugentobler U (2013) The IGS MGEX Experiment as a milestone for a comprehensive multi-GNSS service. In: *Proceedings of ION-PNT-2013*, Honolulu, USA, 22–25 April
- Satirapod C, Luansang M (2008) Comparing stochastic models used in GPS precise point positioning. *Surv Rev* 40(308):188–194. doi:10.1179/003962608X290988
- Schaffrin B, Grafarend E (1986) Generating classes of equivalent linear models by nuisance parameter elimination, applications to GPS observations. *Manuscr Geod* 11:262–271
- Schönemann E, Becker M, Springer T (2011) A new approach for GNSS analysis in a multi-GNSS and multi-signal environment. *J Geod Sci* 1(3):204–214
- Simsy A (2006) Three’s the charm: triple-frequency combinations in future GNSS. *InsideGNSS*:38–41, July/August
- Tang W, Deng C, Shi C, Liu J (2014) Triple-frequency carrier ambiguity resolution for Beidou navigation satellite system. *GPS Solut* 18(3):335–344. doi:10.1007/s10291-013-0333-9
- Tegeedor J, Øvstedal O (2014) Triple carrier precise point positioning (PPP) using GPS L5. *Surv Rev* 46(337):288–297. doi:10.1179/1752270613Y.0000000076
- Teunissen PJG, Joosten P, Tiberius C (2002) A comparison of TCAR, CIR and LAMBDA GNSS ambiguity resolution. In: *Proceedings of the ION GPS-2002*, pp 2799–2808, Portland, OR, 24–27 September
- Vollath U, Birnbach S, Landau H (1998) Analysis of three carrier ambiguity resolution (TCAR) technique for precise relative positioning in GNSS-2. In: *Proceedings of ION GPS-98*, pp 417–426, Nashville, TN, 15–18 September
- Wang J, Satirapod C, Rizos C (2002) Stochastic assessment of GPS carrier phase measurements for precise static relative positioning. *J Geod* 76(2):95–104. doi:10.1007/s00190-001-0225-6
- Wu J, Wu S, Hajj G, Bertiger W, Lichten S (1993) Effects of antenna orientation on GPS carrier phase. *Manuscr Geod* 18:91–98
- Xu G (2007) *GPS: theory, algorithms and applications*, 2nd edn. Springer, Berlin
- Zhang X, He X (2015) Performance analysis of triple-frequency ambiguity resolution with BeiDou observations. *GPS Solut* (online). doi:10.1007/s10291-014-0434-0
- Zhang X, Li P (2015) Benefits of the third frequency signal on cycle slip correction. *GPS Solut* (online). doi:10.1007/s10291-015-0456-2
- Zhang X, Liu J, Forsberg R (2006) Application of precise point positioning in airborne survey (in Chinese). *Geomat Inform Sci Wuhan Univ* 31(1):19–22
- Zhao Q, Sun B, Dai Z, Hu Z, Shi C, Liu J (2015) Real-time detection and repair of cycle slips in triple-frequency GNSS measurements. *GPS Solut* 19(3):381–391. doi:10.1007/s10291-014-0396-2